Optimized aperiodic multilayer structures for use as narrow-angular absorbers

Christopher H. Granier, Francis O. Afzal, Simón G. Lorenzo, Mario Reyes Jr., Jonathan P. Dowling, and Georgios Veronis

---

Optimized aperiodic multilayer structures for use as narrow-angular absorbers

Christopher H. Granier,[1,a)] Francis O. Afzal,[2,3] Simón G. Lorenzo,[1,2] Mario Reyes, Jr.,[2,4] Jonathan P. Dowling,[1] and Georgios Veronis[2,5]

[1]*Department of Physics and Astronomy, Hearne Institute of Theoretical Physics, Louisiana State University, Baton Rouge, Louisiana 70803, USA*
[2]*Center for Computation and Technology, Louisiana State University, Baton Rouge, Louisiana 70803, USA*
[3]*Department of Physics, Truman State University, Kirksville, Missouri 63501,USA*
[4]*Department of Physics, California State University, San Bernardino, California 92407, USA*
[5]*School of Electrical Engineering and Computer Science, Louisiana State University, Baton Rouge, Louisiana 70803, USA*

In this paper, we investigate aperiodic multilayer structures for use as narrow-angular absorbers. The layer thicknesses and materials are optimized using a genetic global optimization algorithm coupled to a transfer matrix code to maximize the angular selectivity in the absorptance at a single or multiple wavelengths. We first consider structures composed of alternating layers of tungsten and silicon or silica, and find that it is not possible to achieve angular selectivity in the absorptance with such structures. We next consider structures composed of alternating layers of silicon and silica, and show that when optimized they exhibit high angular selectivity in absorptance. In addition, as the angular selectivity in absorptance increases, the wavelength range of high angular selectivity also decreases. Optimizing the material composition of the multilayer structures, in addition to optimizing the layer thicknesses, leads to marginal improvement in angular selectivity. Finally, we show that by optimizing the absorptance of the multilayer structures at multiple wavelengths, we can obtain structures exhibiting almost perfect absorptance at normal incidence and narrow angular width in absorptance at these wavelengths. Similar to the structures optimized at a single wavelength, the wavelength range of high angularly selective absorptance is narrow.
© 2014 AIP Publishing LLC. [http://dx.doi.org/10.1063/1.4904905]

I. INTRODUCTION

The absorptance properties of materials and structures have been widely investigated in recent years. Bulk materials, such as tungsten, exhibit broadband and broad-angle absorption spectra which vary from material to material. However, it has been demonstrated that the absorption spectra of bulk materials can be drastically changed by using multilayer structures,[1] textured surfaces, or other three dimensional constructions.[2,3] Several different structures with modified absorptance properties have been investigated, including metallic gratings,[4,5] metallic and semiconductor photonic crystals,[6–8] periodic grooves,[9] and nano-antennae.[10] The use of metamaterials has also been investigated as a possible method for tailoring the absorptance characteristics.[11] Developing such structures that have unusual absorption characteristics in the optical wavelength range is important for many applications such as photovoltaics,[12–14] control of thermal radiation,[15,16] photodetectors,[17,18] and chemical sensing.[7,19]

Most related efforts have been focused on developing structures with wide-angle near-perfect absorption in either a narrow or a broad wavelength range.[20–29] However, structures which exhibit angular selectivity in absorptance are also investigated because of their many potential applications.[30,31] In particular, in solar thermophotovoltaics solar radiation is absorbed by an intermediate absorber, which then emits thermal radiation towards a solar cell. Solar thermophotovoltaic cells are capable of achieving theoretical efficiency which far exceeds the Shockley-Queisser limit when a single-junction cell is directly exposed to sunlight.[14,32] In order to approach such efficiency, however, there are very important constraints on the properties of the intermediate absorber. For efficient solar thermophotovoltaic systems which do not employ sunlight concentration, the intermediate absorber must exhibit broadband angular selectivity. More specifically, it must provide near-perfect absorption in a narrow angular range, corresponding to the solid angle subtended by the Sun, over the entire solar spectrum.[14,32,33] Efficient solar thermophotovoltaic systems must have relatively high temperature.[33] From the Earth's surface, the solid angle subtended by the Sun is very small. However, a conventional planar surface emits radiation isotropically in all 2π steradians. Due to this angular mismatch, the planar surface reaches thermal equilibrium at a much lower temperature than the Sun's temperature. Angular selectivity in the absorption of the intermediate absorber is therefore highly desired in the case of no sunlight concentration,[32,33] since then we can avoid the loss of energy by the radiation of the intermediate radiator outside of the solid angle subtended by the Sun, a process which cools the absorber. It was also recently demonstrated that it is possible to design structures which exhibit broadband angular selectivity in transmission

a)Electronic mail: cgrani1@lsu.edu

by tailoring the overlap of the band gaps of multiple photonic crystals, so as to preserve the characteristic Brewster modes in a broad wavelength range.[34]

In this paper, we investigate one-dimensional multilayer aperiodic structures for use as narrow-angular absorbers. It has been demonstrated that multilayer structures can tailor the absorptance spectra of bulk materials.[35] In many cases, a multilayer structure may provide spectra-altering properties similar to that of more complex and harder-to-fabricate two- or three-dimensional structures. Here, we optimize the layer thicknesses and materials using a genetic global optimization algorithm coupled to a transfer matrix code to maximize the angular selectivity in the absorptance at a single or multiple wavelengths. We first consider structures composed of alternating layers of tungsten and silicon or silica over a tungsten substrate. We find that, due to the high absorption of tungsten, it is not possible to achieve angular selectivity in the absorptance with such structures. We next consider structures composed of alternating layers of silicon and silica. Unlike the structures containing tungsten, the optimized silicon-silica structures exhibit high angular selectivity in absorptance at the wavelength at which they are optimized. However, as the angular selectivity in absorptance increases, the wavelength range of high angular selectivity decreases. We then consider optimizing the material composition of the multilayer structures, in addition to optimizing the layer thicknesses, and find that this approach leads to marginal improvement in angular selectivity when compared to the silicon-silica structures. Finally, we investigate optimizing the absorptance of the multilayer structures at multiple wavelengths. We find that with this approach we can obtain structures exhibiting almost perfect absorptance at normal incidence and narrow angular width in absorptance at these wavelengths. However, similar to the structures optimized at a single wavelength, the wavelength range of high angularly selective absorptance is narrow.

We previously showed that optimized aperiodic multilayer structures can lead to narrowband, highly directional thermal infrared emitters.[36] In this work, structures are designed to operate in the visible. We note that the properties of the materials used are very different in these two wavelength ranges. Silicon is essentially lossless in the infrared, while it is quite lossy in the visible. As a result, the mechanisms that lead to high angular selectivity in absorptance are very different. In the infrared designs, all the power is absorbed in the tungsten substrate.[36] In the visible designs presented in this work only a portion of the power is absorbed in the substrate. In fact, in some of the designs almost no power is absorbed in the substrate. One can think of such structures as lossy multilayer resonators which are almost perfectly impedance matched to air. In this work, we also show that it is not possible to achieve angular selectivity in the absorptance with structures composed of alternating layers of metals, such as tungsten, and dielectrics due to the high material loss of metals. In addition, we investigate the effect of optimizing the material composition of multilayer structures, in addition to optimizing the layer thicknesses. Finally, we show that with the proposed aperiodic structures it is possible to achieve almost perfect absorptance at normal

incidence and narrow angular width in absorptance at multiple closely spaced tunable wavelengths.

The remainder of this manuscript is divided into three sections. The computational techniques used will be discussed in Sec. II. The results are described in Sec. III, which is subdivided into four subsections. Subsection III A discusses the results of genetic-algorithm optimized structures composed of tungsten and silicon as well as tungsten and silica. Subsection III B presents the results of genetic-algorithm optimized silicon-silica structures for use as angular selective absorbers. In Subsection III C, we investigate optimizing the material composition of the multilayer structures, in addition to optimizing the layer thicknesses. Subsection III D presents genetic-algorithm-optimized aperiodic structures composed of alternating layers of silicon and silica with narrow angular absorptance at two wavelengths (a narrow-angular, bichromatic absorber). Our conclusions are summarized in Sec. IV.

II. THEORY

We model an aperiodic structure composed of infinite slabs of material of varying thicknesses, as depicted in Fig. 1. Light is incident from air at an angle θ to the structure. Utilizing the transfer matrix method,[37] we calculate the transmittance, reflectance, and absorptance of the structure for both TE (transverse electric) and TM (transverse magnetic) polarized light. We make use of experimental data for the wavelength-dependent indices of refraction, both real and imaginary parts, for silicon carbide, silica, silicon, and tungsten[38] for the calculations done in this paper. These materials are commonly used in applications related to engineering the absorptance properties of different structures,[14,39] and have high melting points. In addition, silicon and silica provide a high index contrast which is useful for engineering the photonic band structure. It is important to note that in the visible range of wavelengths, both silica and silicon carbide are almost lossless. Since the tungsten substrate is taken to be semi-infinite, the transmittance is identically zero, so that

$$A_{\text{TE/TM}}(\lambda, \theta) = 1 - R_{\text{TE/TM}}(\lambda, \theta), \quad (1)$$

where $A_{\text{TE/TM}}$ is the TE/TM absorptance, $R_{\text{TE/TM}}$ is the TE/TM reflectance, and λ is the wavelength.

We are interested in finding structures which are highly absorbing for normally incident light and also exhibit highly directional absorptance.

We use a genetic optimization algorithm to determine the best structure's dimensions for varying numbers of layers at a given wavelength λ_0. The implementation of the genetic algorithm that we use has been realized in-house. A genetic algorithm is an iterative optimization procedure, which starts with a randomly selected population of potential solutions, and gradually evolves toward improved solutions, via the application of the genetic operators. These genetic operators are patterned after the natural selection process. In the initialization function, a population of chromosomes is created by random selection of values for the genes. The genetic
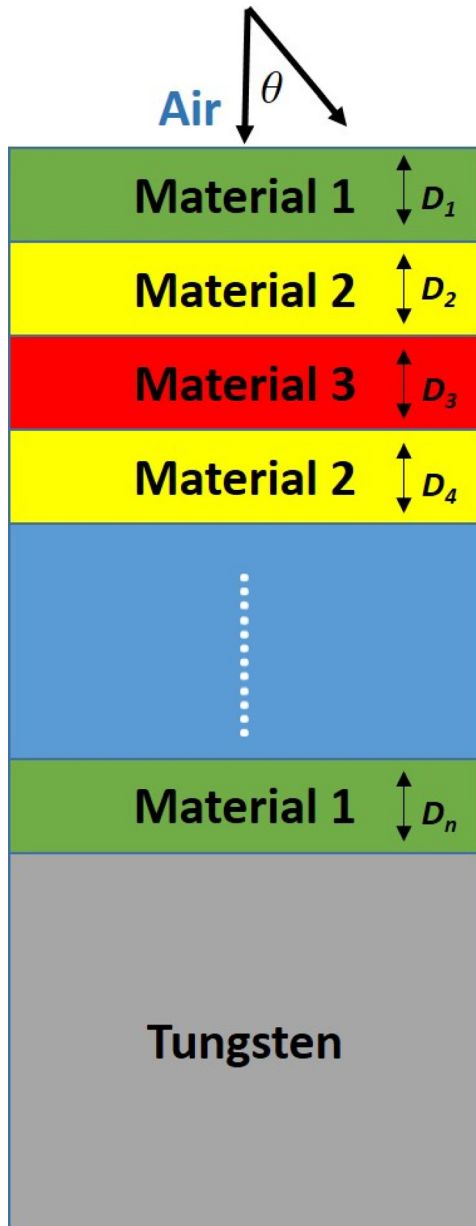
FIG. 1. Schematic of aperiodic structure optimized by genetic algorithm coupled to the transfer matrix code. Incident light at an angle θ to the normal of the surface of the structure enters the n-layer structure comprised of various materials above a semi-infinite tungsten substrate.

algorithm then proceeds to iteratively generate a new population by the application of selection, crossover, and mutation operators.

More specifically, here, we use the microgenetic algorithm. It has been shown that the microgenetic algorithm avoids premature convergence and shows faster convergence to the near-optimal region compared to the conventional large-population genetic algorithm for multidimensional problems.[40–42] The microgenetic algorithm starts with a small random population which evolves and converges after a few generations. At this point, keeping the best individual from the previously converged generation, a new random population is chosen, and the evolution process restarts.

We use the tournament selection as the selection scheme in the genetic algorithm. In this method, a subpopulation of individuals is randomly chosen from the population and made to compete on the basis of their fitness values. The individual in the subpopulation with the highest fitness value wins the tournament, and is thus selected. The remaining members of the entire subpopulation are then put back into the general population, and the process is repeated. This selection scheme converges more rapidly and has a faster execution time compared to other competing schemes.[43] Once a pair of individuals is selected as parents, the basic crossover operator creates two offspring by combining the chromosomes of their parents. We use uniform crossover rather than single point crossover, as it has been found that microgenetic algorithm convergence is faster with the uniform crossover.[41,43] An elitist strategy is also employed, wherein the best individual from one generation is passed on to the next generation.

Specifically, for the structures discussed in Subsections III A–III C, we calculate the absorptance of each structure as a function of angle for $0° \leq \theta \leq 90°$ at wavelength λ_0. We then minimize the fitness function, $F(\lambda_0)$

$$F(\lambda_0) = \int_0^{\frac{\pi}{2}} A_{\text{Total}}(\lambda_0, \theta)\, d\theta, \qquad (2)$$

subject to the constraint that $A_{\text{Total}}(\lambda_0, \theta = 0°) \geq A_{\min}$. Here, $A_{\text{Total}}(\lambda_0, \theta) = [A_{\text{TE}}(\lambda_0, \theta) + A_{\text{TM}}(\lambda_0, \theta)]/2$. That is, we calculate the integral of the absorptance over all angles θ at a given wavelength, λ_0, and minimize it subject to the constraint that the absorptance at normal incidence is at least $A_{\min}$.

III. RESULTS

In this section, we discuss genetic-algorithm-optimized structures for use as directional absorbers. Each structure is optimized for angular selectivity in an attempt to find a broadband, narrow-angle absorber. The structures discussed in Subsections III A–III C are optimized at $\lambda_0 = 550\,\text{nm}$, roughly the center of the visible range. The structure discussed in Subsection III D is optimized to operate as a narrow-angular, bichromatic absorber. It is optimized at both $\lambda_1 = 450\,\text{nm}$ and $\lambda_2 = 550\,\text{nm}$, which correspond to indigo and green light, respectively, in the visible range.

A. Tungsten-silicon and tungsten-silica structures

Using the transfer matrix method and genetic algorithm as outlined in Sec. II, we investigate the properties of the aperiodic one-dimensional structures. We choose $\lambda_0 = 550\,\text{nm}$ at the center of the visible spectrum as the wavelength at which to optimize angular selectivity of the absorptance.

First, we consider structures of six, eight, and sixteen layers composed of alternating layers of tungsten and silicon over a semi-infinite tungsten substrate. In each case, we minimize the fitness function, $F(\lambda_0)$, [Eq. (2)] subject to the constraint that the normal incidence absorptance, $A_{\text{Total}}(\lambda_0, \theta) \geq A_{\min} = 0.90$. For comparison of the structures, we define the angular full width at half maximum
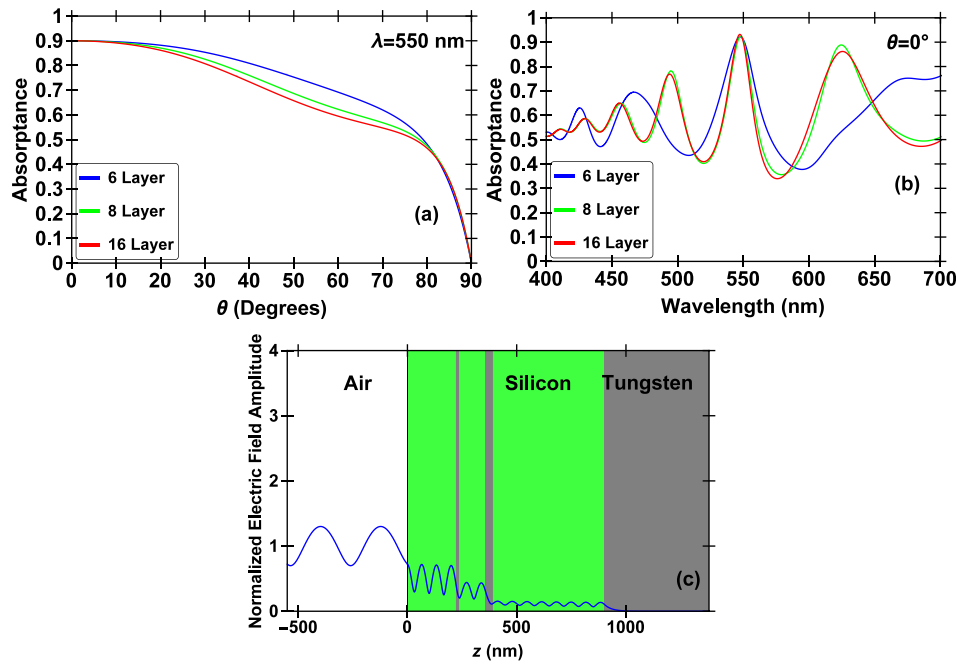
FIG. 2. (a) Absorptance versus angle of an optimized, aperiodic multilayer structure of six, eight, and sixteen alternating layers of tungsten and silicon over a semi-infinite tungsten substrate. The structure is optimized such that the integral of the absorptance over all angles for $\lambda_0 = 550$ nm is minimized subject to the constraint that the absorptance at normal incidence is greater than 90% ($A_{min} = 0.90$). The layer thicknesses of the optimized tungsten-silicon structures (in units of nanometers) are: {0, 222, 17, 117, 34, 511} for the six-layer structure, {0, 357, 17, 51, 18, 48, 30, 313} for the eight-layer structure, and {0, 166, 0, 37, 0, 154, 17, 51, 17, 56, 15, 50, 26, 43, 34, 443} for the sixteen-layer structure. It is important to note that, for some layers, the optimized thickness was found to be zero. We found that for the optimized tungsten-silicon structures the top layer, which is adjacent to air, is always silicon. (b) Absorptance versus wavelength of the same structures described in (a) at normal incidence. (c) Profile of the electric field amplitude, normalized with respect to the field amplitude of the incident plane wave for the six-layer genetic-algorithm-optimized tungsten-silicon aperiodic structure described in (a). Note that the thickness of the first tungsten layer is zero; thus, the layer adjacent to air is silicon. The structure is excited by a normally incident plane wave at the wavelength of $\lambda_0 = 550$ nm. The ratio of the power absorbed inside each layer to the total power absorbed in the structure was calculated and from left to right, beginning with air, is: {0, 0.273, 0.323, 0.06, 0.274, 0.03, 0.04}. That is, ~27.3% of the power is absorbed in the first silicon layer adjacent to air; while, ~4% is absorbed in the tungsten substrate.

(FWHM), $\delta\theta_n$, for the n-layer structure, calculating the width about $\theta = 0°$, for which the absorptance is larger than half of the maximum achieved value, as seen in Fig. 2(a). We also define the spectral FWHM, $\delta\lambda_n$, for the n-layer structure, calculating the width about the wavelength at which we optimized the structure, λ_0, for which the absorptance is larger than half of the maximum achieved value, as seen in Fig. 2(b). These results for the tungsten-silicon structure are found in Table I.

We observe that the genetic-algorithm-optimized tungsten-silicon structures do not exhibit angular selectivity [Fig. 2(a)]. In addition, the structures exhibit no wavelength-selectivity and the absorptance is relatively broadband in nature. The structures exhibit absorptance of more than 50% in a broad wavelength range [Fig. 2(b)]. There is very little change in the angular FWHM, $\delta\theta_n$, of the respective silicon-tungsten genetic-algorithm-optimized structures with increasing number of layers (Table I). Overall, the silicon-tungsten material combination fails to provide angular selectivity and increasing number of layers does not improve the

TABLE I. Angular FWHM $\delta\theta_n$ and spectral FWHM $\delta\lambda_n$ of the tungsten-silicon structures described in Fig. 2(a).

n	$\delta\theta_n$	$\delta\lambda_n$ (nm)
6	161.4°	70.4
8	161.6°	42.6
16	161.8°	45.4

angular selectivity. This is due to the high absorption of tungsten. In Fig. 2(c), we show the profile of the electric field amplitude, normalized with respect to the field amplitude of the incident plane wave for the six-layer genetic-algorithm-optimized aperiodic tungsten-silicon structure. The structure is excited by a normally incident plane wave at the wavelength of $\lambda_0 = 550$ nm. We observe that the structure is almost perfectly impedance-matched to air, since only ~10% of the incident power is reflected. For this tungsten-silicon structure, the first two layers provide the majority of the absorption in the structure, contributing ~27% and ~32%, respectively. The second tungsten layer provides ~27%; while, the substrate provides less than ~5% of the overall absorption of the structure. In the silicon-tungsten structure, it is obvious from Fig. 2(c) that there is no field enhancement provided by the structure. We therefore conclude that the high absorptance at normal incidence is not associated with any strong resonances. This is also supported by the broad angle and wideband absorptance depicted in Figs. 2(a) and 2(b).

We also consider structures of six, eight, and sixteen layers composed of alternating layers of tungsten and silica. Again, we minimize the fitness function, $F(\lambda_0)$, [Eq. (2)] subject to the constraint that the normal incidence absorptance, $A_{Total}(\lambda_0, \theta) \geq A_{min} = 0.90$.

Similar to the tungsten-silicon structures, the tungsten-silica structures do not exhibit high angular selectivity in absorptance. As depicted in Fig. 3(a), the tungsten-silica
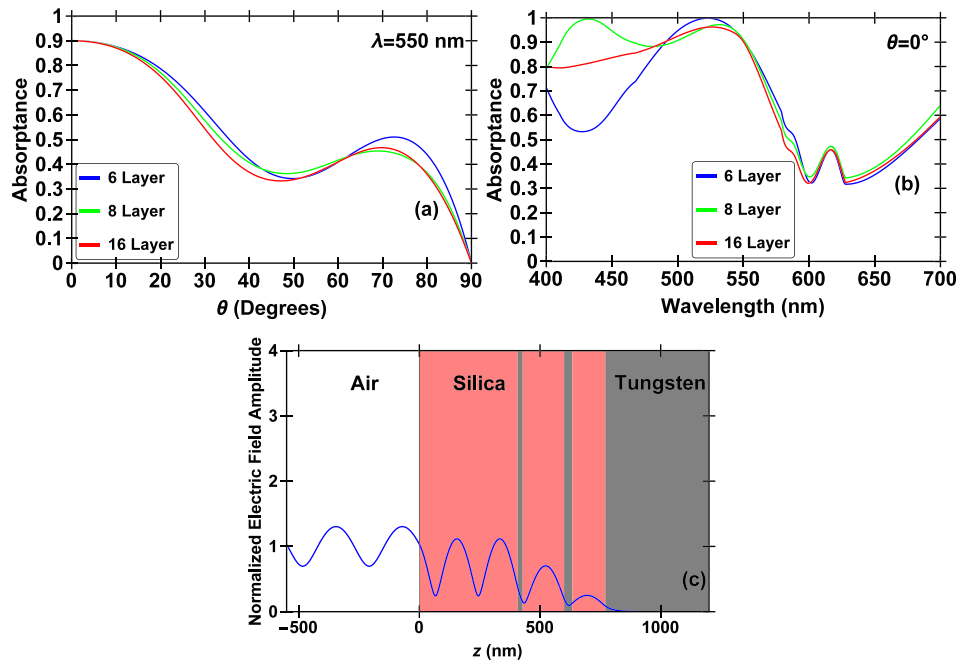
FIG. 3. (a) Absorptance versus angle of an optimized aperiodic multilayer structure of six, eight, and sixteen alternating layers of tungsten and silica over a semi-infinite tungsten substrate. The structure is optimized such that the integral of the absorptance over all angles for $\lambda_0 = 550$ nm is minimized subject to the constraint that the absorptance at normal incidence is greater than 90% ($A_{min} = 0.90$). The layer thicknesses of the optimized tungsten-silica structures (in units of nanometers) are: {2, 406, 21, 171, 34, 137} for the six-layer structure, {0, 395, 3, 207, 21, 165, 34, 144} for the eight-layer structure, and {0, 413, 9, 192, 22, 168, 22, 155, 26, 293, 0, 392, 17, 163, 13, 517} for the sixteen-layer structure. It is important to note that, for some layers, the optimized thickness was found to be zero. We also found that for the optimized tungsten-silicon structures the top layer, which is adjacent to air, is in the case of the eight and sixteen layer structure, silicon. (b) Absorptance versus wavelength of the same structures described in (a) at normal incidence. (c) Profile of the electric field amplitude, normalized with respect to the field amplitude of the incident plane wave for the six-layer genetic-algorithm-optimized tungsten-silica aperiodic structure described in (a). The structure is excited by a normally incident plane wave at the wavelength of $\lambda_0 = 550$ nm. The ratio of the power absorbed inside each layer to the total power absorbed in the structure was calculated and from left to right, beginning with air, is: {0, 0.541, 0, 0.302, 0, 0.13, 0, 0.03}. That is, ~54.1% of the power is absorbed in the first tungsten layer adjacent to air; while, ~3% is absorbed in the tungsten substrate.

structures all achieve a peak of 90% absorptance at normal incidence and exhibit reduced angular FWHM, $\delta\theta_n$, (Table II) when compared to the tungsten-silicon structures. However, the tungsten-silica structures maintain high absorptance for large angles of incidence [Fig. 3(a)]. We note that the tungsten-silica structures possess more broadband absorptance having a larger spectral FWHM ($\delta\lambda_n$) compared to the tungsten-silicon structures (Table II). In Fig. 3(c), we show the profile of the electric field amplitude, normalized with respect to the field amplitude of the incident plane wave for the six-layer genetic-algorithm-optimized aperiodic tungsten-silica structure. As before, the structure is excited by a normally incident plane wave at the wavelength of $\lambda_0 = 550$ nm. In the tungsten-silica structure, ~85% of the absorption occurs in the first two tungsten layers. The substrate provides less than ~5% of the overall absorptance in the structure. As with the tungsten-silicon structure, the absorptance mechanism is non-resonant and is the result of impedance matching.

Overall, due to the high absorption of tungsten, we found that it is not possible to achieve angular selectivity with structures using tungsten. In both tungsten-based structures, the high absorptance at normal incidence is not associated with resonant field enhancement. In addition, in both cases, the structures were impedance-matched to air in a broad wavelength range.

B. Silica-silicon structures

We consider structures of four, six, eight, and sixteen layers composed of alternating layers of silicon and silica over a semi-infinite tungsten substrate. In each case, we minimize the fitness function, $F(\lambda_0)$, [Eq. (2)] subject to the constraint that the normal incidence absorptance at $\lambda_0 = 550$ nm $A_{Total}(\lambda_0, \theta) \geq A_{min} = 0.95$. In doing so, we seek structures which provide narrow angular absorptance profiles.

The genetic-algorithm-optimized, silicon-silica structures exhibit angular selectivity at $\lambda = 550$ nm, the wavelength at which the structures are optimized. As before, the FWHM comparison of the optimized four, six, eight, and sixteen layer structures can be found in Table III. All of the silicon-silica structures exhibit angular selectivity, with each structure peaking at 95% absorptance at normal incidence and decreasing rapidly as θ increases [Fig. 4(a)]. We also note that there is a trend of increasing angular selectivity as the number of layers increases. For comparison, the

TABLE II. Angular FWHM $\delta\theta_n$ and spectral FWHM $\delta\lambda_n$ of the tungsten-silica structures described in Fig. 3(a).

n	$\delta\theta_n$	$\delta\lambda_n$ (nm)
6	74.6°	88.4
8	72.9°	82.6
16	68.4°	71.0

TABLE III. Angular FWHM $\delta\theta_n$ and spectral FWHM $\delta\lambda_n$ of the silicon-silica structures described in Fig. 4(a).

n	$\delta\theta_n$	$\delta\lambda_n$ (nm)
4	28.8°	12.8
6	20.8°	6.6
8	13.3°	2.6
16	6.9°	0.8

absorptance of bulk tungsten at this wavelength is also shown. Fig. 4(b) shows the spectral response at normal incidence of the six-layer genetic-algorithm-optimized, silicon-silica structure as well as bulk-tungsten's response. The six-layer structure provides a narrow band response centered close to the wavelength at which it is optimized with additional resonances at other wavelengths. The eight and sixteen layer structures' spectral response at normal incidence is similar. As the number of layers in the optimized structure increases, the number of resonances in the $\lambda = 400$ nm to $\lambda = 700$ nm wavelength range also increases. Fig. 4(c) shows the absorptance of the four, six, eight, and sixteen layer structures near $\lambda = 550$ nm, the wavelength at which the structures are optimized. We observe that there is a trend of decreasing spectral resonance width with increasing number of layers in the optimized structure. Fig. 5 shows a color plot of the absorptance as a function of both angle and wavelength for the eight-layer, genetic-algorithm-optimized structure. We observe that the

structure exhibits angular selectivity around the wavelength at which it was optimized, but its angular occurrence shifts with wavelength. More specifically, as the wavelength decreases, the peak of the absorptance shifts to larger angles. Overall, with increasing number of layers, we observe an increase in angular selectivity and a decrease in the wavelength range of high absorptance at normal incidence.

In Fig. 6, we show the profile of the electric field amplitude, normalized with respect to the field amplitude of the incident plane wave for both the six-layer and eight-layer genetic-algorithm-optimized, silicon-silica aperiodic structures. The structure is excited by a normally incident plane wave at $\lambda_0 = 550$ nm, the wavelength at which the structures are optimized. In the six-layer structure [Fig. 6(a)], we observe a large, resonant enhancement of the electric field toward the center of the structure. As a result, the majority ($\sim$77%) of the power is absorbed in the tungsten substrate. In the eight-layer structure [Fig. 6(b)], the enhancement of the field is approximately twice the enhancement of the six-layer structure; however, the majority of the power is absorbed outside of the tungsten substrate. Less than one-third of the overall power is absorbed in the tungsten substrate. The two largest contributors to power absorbed for the eight-layer structure are the second and third silicon layers with the second silicon layer absorbing $\sim$29% and the third silicon layer absorbing $\sim$32% of the total power absorbed by the structure. Overall, we found that with increasing number of layers, the fraction of the power absorbed in the substrate
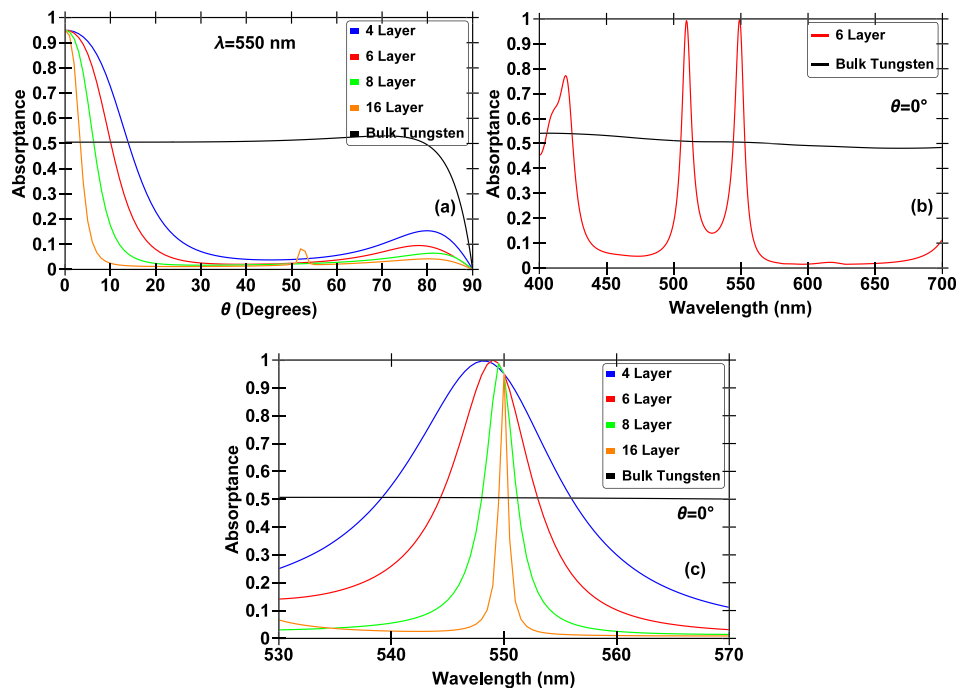

FIG. 4. (a) Absorptance versus angle of an optimized aperiodic multilayer structure of four, six, eight, and sixteen alternating layers of silicon and silica over a semi-infinite tungsten substrate. The structure is optimized such that the integral of the absorptance over all angles for $\lambda_0 = 550$ nm is minimized subject to the constraint that the absorptance at normal incidence is greater than 0.95 ($A_{min} = 0.95$). The absorptance of bulk tungsten is depicted in black for reference. The layer thicknesses of the optimized silicon-silica structures (in units of nanometers) are: {28, 530, 33, 301} for the four-layer structure, {30, 508, 32, 340, 34, 88} for the six-layer structure, {25, 110, 34, 530, 34, 92, 33, 80} for the eight-layer structure, and {12, 172, 28, 120, 34, 496, 34, 503, 0 (silicon), 550, 25, 321, 27, 106, 36, 81} for the sixteen-layer structure. It is important to note that in some cases the optimized thickness was found to be zero. (b) Absorptance versus wavelength of the six-layer structure described in (a) at normal incidence. Again, absorptance of bulk tungsten is depicted in black for reference. (c) Absorptance versus wavelength of the four, six, eight, and sixteen layer structures zoomed in on the wavelength for which the structure was optimized. Absorptance of bulk tungsten is depicted in black for reference.
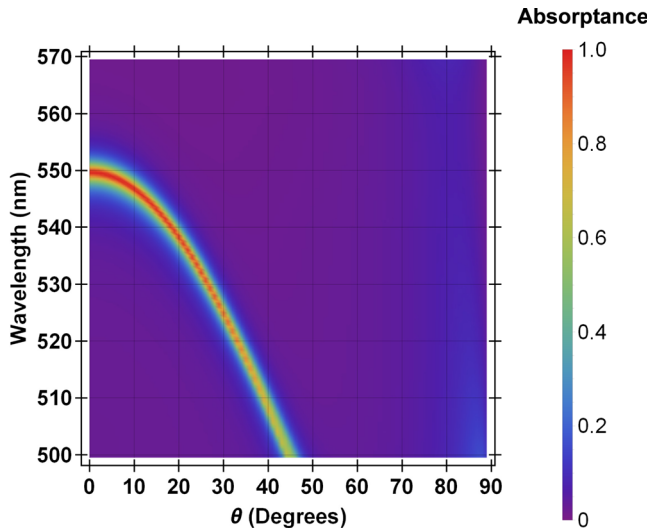
FIG. 5. Absorptance as a function of wavelength and angle for the eight-layer, genetic-algorithm-optimized, aperiodic structure described in Fig. 4(a).

decreases. We also found that when the wavelength or the angle of incidence is shifted away from the resonance the field enhancement rapidly decreases. This is consistent with the narrowband, highly directional absorptance of the structure (Fig. 4). Additionally, it is important to note that as the number of layers increases, the field enhancement drastically increases.

In short, unlike the structures containing tungsten, optimized, multilayer, silicon-silica structures exhibit high angular selectivity for absorptance at the wavelength at which they are optimized. However, we found that, for such optimized multilayer silicon-silica structures, as the angular FWHM, $\delta\theta_n$, decreases, the spectral FWHM, $\delta\lambda_n$, also decreases. In other words, as the angular selectivity in absorptance increases, the wavelength range of high angular selectivity decreases.

C. Multiple material structures

We also investigated optimizing the material composition of the multilayer structures in addition to optimizing the layer thicknesses. As before, we minimize the fitness function, $F(\lambda_0)$, [Eq. (2)] subject to the constraint that the normal incidence absorptance at $\lambda_0 = 550$ nm $A_{Total}(\lambda_0, \theta) \geq A_{min} = 0.95$. In doing so, we seek structures which provide narrow angular absorptance profile. More specifically, for each layer, the material was chosen among silicon, silica, tungsten, and silicon carbide. In each case, the genetic optimization algorithm searched for the optimal material composition as well as the optimal thickness of each layer. We considered structures consisting of four, six, eight, and sixteen layers. In all cases except for the four-layer structure, silicon carbide was found to be the optimal material for the first layer adjacent to air. In addition, none of the optimized multilayer structures contained tungsten. The fact that the optimal material composition of the multilayer structure does not contain tungsten is consistent with our conclusion in Subsection III A that it is not possible to achieve angular selectivity in the absorptance with structures containing highly lossy materials such as tungsten.

Even though the optimized material composition was found to be, in general, different from the one of the silicon-silica multilayer structures, the improvement in angular selectivity with respect to silicon-silica structures with the same number of layers was marginal. More specifically, for a given number of layers n, the angular FWHM, $\delta\theta_n$ of the structures with optimized material composition was no more than 2% decreased with respect to the silicon-silica multilayer structures with the same number of layers.

D. Bichromatic absorber

As described in Subsection III B, optimized silicon-silica multilayer structures exhibit high angular selectivity in absorptance when optimized at a single wavelength in the
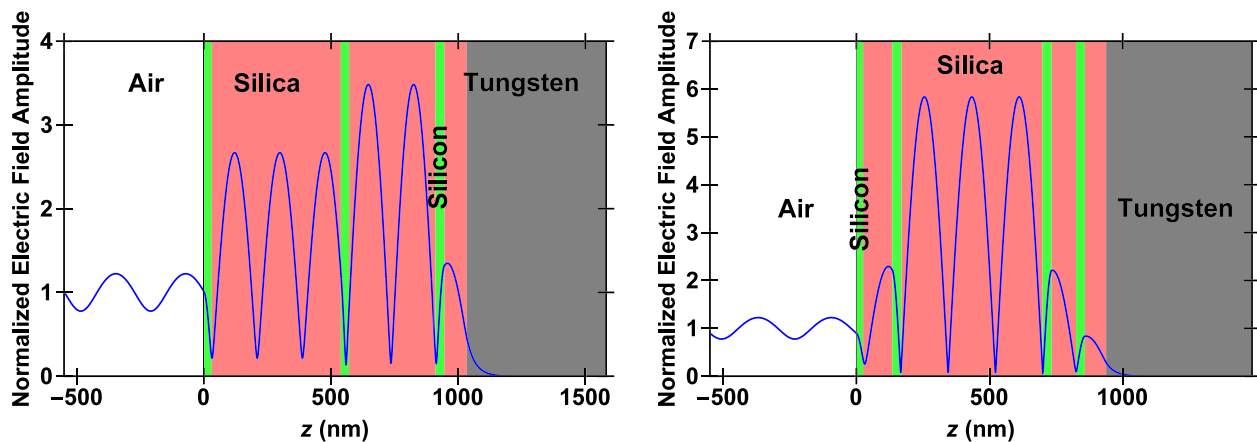

FIG. 6. (a) Profile of the electric field amplitude, normalized with respect to the field amplitude of the incident plane wave for the six-layer genetic-algorithm-optimized aperiodic structure described in Fig. 4(a). The structure is excited by a normally incident plane wave at the wavelength of $\lambda_0 = 550$ nm. The ratio of the power absorbed inside each layer to the total power absorbed in the structure was calculated and from left to right, beginning with air, is: {0, 0.062, 0, 0.06, 0, 0.107, 0, 0.77}. (b) Profile of the electric field amplitude, normalized with respect to the field amplitude of the incident plane wave for the eight-layer genetic-algorithm-optimized aperiodic structure described in Fig. 4(a). The structure is excited by a normally incident plane wave at the wavelength of $\lambda_0 = 550$ nm. The ratio of the power absorbed inside each layer to the total power absorbed in the structure was calculated and from left to right, beginning with air, is: {0, 0.048, 0, 0.29, 0, 0.318, 0, 0.046, 0, 0.3}. That is, ~5% of the power is absorbed in the first silicon layer adjacent to air; while, ~30% is absorbed in the tungsten substrate.

visible wavelength range. However, as the angular selectivity increases, wavelength selectivity also increases. In an attempt to increase the wavelength range of high angular selectivity in absorptance, we investigate optimizing the angular selectivity of multilayer structures at multiple wavelengths.

More specifically, we calculate the absorptance of each structure as a function of angle for $0° \leq \theta \leq 90°$ at two wavelengths, $\lambda_1 = 450$ nm and $\lambda_2 = 550$ nm in the visible wavelength range. Then we minimize the fitness function, $F_1(\lambda_1, \lambda_2)$

$$F_1(\lambda_1, \lambda_2) = \int_0^{\frac{\pi}{2}} [A_{\text{Total}}(\lambda_1, \theta) + A_{\text{Total}}(\lambda_2, \theta)] \, d\theta, \quad (3)$$

subject to the constraints $A_{\text{Total}}(\lambda_i, \theta = 0°) \geq A_{\min} = 0.95$, $i = 1, 2$. Here, $A_{\text{Total}}(\lambda_i, \theta) = [A_{\text{TE}}(\lambda_i, \theta) + A_{\text{TM}}(\lambda_i, \theta)]/2$.

That is, we calculate the integral of the sum of the absorptances at the wavelengths at which the structure is optimized over all angles, θ, and minimize it subject to the constraint that the absorptance at normal incidence is at least $A_{\min} = 0.95$ at all wavelengths considered. However, we found that with this optimization process, the absorptance response of the optimal structures was not unique. This is due to the fact that structures with identical fitness, $F_1(\lambda_1, \lambda_2)$ may exhibit different angular selectivity at the wavelengths at which the structures are optimized. As an example, we consider two distinct structures. One of the

structures exhibits higher angular selectivity at wavelength λ_1, $[\delta\theta(\lambda_1) < \delta\theta(\lambda_2)]$; the other one exhibits higher angular selectivity at λ_2 $[\delta\theta(\lambda_1) > \delta\theta(\lambda_2)]$, while both have the same fitness, $F_1(\lambda_1, \lambda_2)$.

To address this, we added one additional constraint in the optimization process

$$F_2(\lambda_1, \lambda_2) = \frac{2}{\pi} \int_0^{\frac{\pi}{2}} |A_{\text{Total}}(\lambda_1, \theta) - A_{\text{Total}}(\lambda_2, \theta)| \, d\theta \leq \epsilon. \quad (4)$$

That is, we constrained the angle-average difference between the absorptances at the two wavelengths at which the structures were optimized to be less than ϵ. Here, we chose $\epsilon = 0.01$. In other words, the average difference in the angular absorptance profiles has to be less than 1%.

Here, we consider a structure composed of eight alternating layers of silicon and silica above a thick tungsten substrate. We found that at least eight layers are required in the silicon-silica structure in order to achieve high angular selectivity at the two wavelengths at which the absorptance of the structure was optimized. The structure provides relatively narrow-angular absorptance features at both of the wavelengths at which it was optimized $\lambda_1 = 450$ nm and $\lambda_2 = 550$ nm. In fact, the angular absorptance spectra for the two wavelengths are nearly identical [Fig. 7(a)]. The absorptance of the optimized structure at normal incidence as a function of wavelength is shown in Fig. 7(b). The
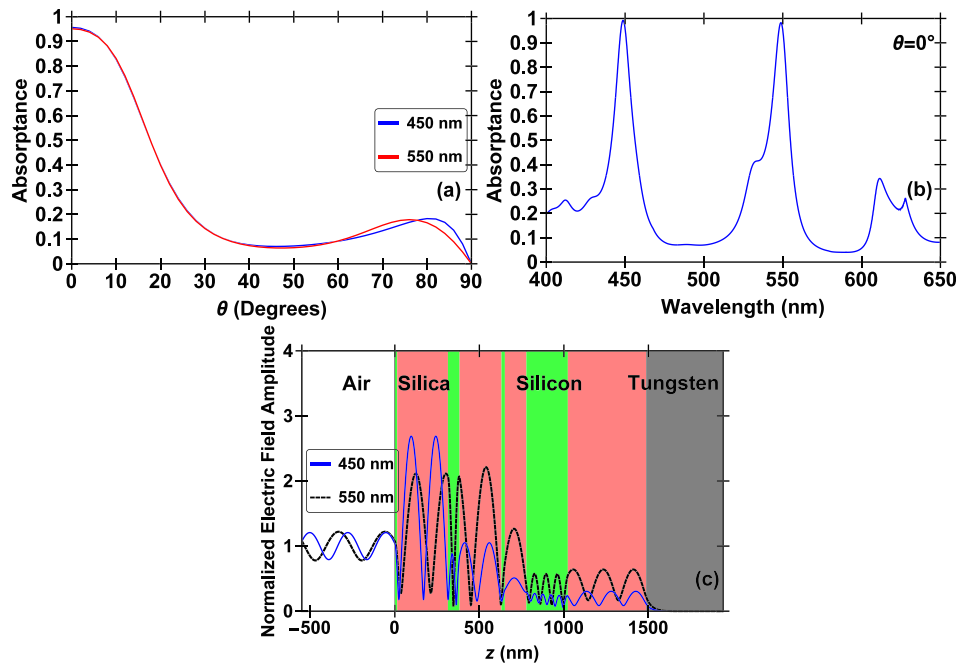

FIG. 7. (a) Absorptance versus angle of an aperiodic multilayer structure of eight alternating layers of silicon and silica over a semi-infinite tungsten substrate. The structure is optimized such that the integral of the sum of the absorptances at the wavelengths at which the structure was optimized over all angles, θ, is minimized subject to the constraint that the absorptance at normal incidence was at least $A_{\min} = 0.95$ at all wavelengths considered. Simultaneously, we constrained the angle-average difference between the absorptances at the two wavelengths at which the structures were optimized to be less than 0.01. The layer thicknesses of the optimized silicon-silica structure (in units of nanometers) for the eight-layer structure are: {14, 300, 69, 248, 21, 127, 245, 463}. (b) Absorptance versus wavelength of the same structure described in (a) at normal incidence. (c) Profile of the electric field amplitude, normalized with respect to the field amplitude of the incident plane wave for the eight-layer, genetic-algorithm-optimized, aperiodic structure described in Fig. 7(a). The structure is excited by a normally incident plane wave of $\lambda_1 = 450$ nm (blue) and $\lambda_2 = 550$ nm (black, dashed). The ratio of the power absorbed inside each layer to the total power absorbed in the structure was calculated and from left to right, beginning with air, is: {0, 0.217, 0, 0.519, 0, 0.025, 0, 0.196, 0, 0.04} for $\lambda_1 = 450$ nm, and {0, 0.053, 0, 0.596, 0, 0.021, 0, 0.155, 0, 0.17} for $\lambda_2 = 550$ nm. That is, for $\lambda_1 = 450$ nm, ~22% of the power is absorbed in the first silicon layer adjacent to air; while, ~4% is absorbed in the tungsten substrate.

TABLE IV. Angular FWHM $\delta\theta_n$ and spectral FWHM $\delta\lambda_n$ of the structures described in Fig. 7(a).

Wavelength (nm)	$\delta\theta$	$\delta\lambda$ (nm)
$\lambda_1 = 450$	$36.7°$	8.4
$\lambda_2 = 550$	$36.6°$	10.6

structure absorbs the incident light almost completely at the two wavelengths at which it was optimized; however, similar to the structures optimized at a single wavelength (Subsection III B), the wavelength range of high angularly selective absorptance is narrow (Table IV).

In Fig. 7(c), we show the profile of the electric field amplitude, normalized with respect to the field amplitude of the incident plane wave for the eight-layer, genetic-algorithm-optimized, aperiodic structure. The structure is excited by a normally incident plane wave at either $\lambda_1 = 450$ nm or $\lambda_2 = 550$ nm. While the wavelengths at which the structure was optimized have nearly identical angular spectra, the two absorptance mechanisms within the structure are different. The $\lambda_1 = 450$ nm light is absorbed mainly in the first two silicon layers, which account for over $\sim 70\%$ of the structure's absorbed power. The tungsten substrate accounts for less than $\sim 5\%$ of the overall power absorbed at $\lambda_1 = 450$ nm. The $\lambda_2 = 550$ nm light is absorbed mostly in the second silicon layer, which provides $\sim 60\%$ of the overall absorption at this wavelength; the final silicon layer before the tungsten substrate and the substrate itself account for an additional $\sim 30\%$ of the structure's absorbed power.

IV. CONCLUSION

We investigated one-dimensional aperiodic multilayer structures for use as narrow-angular absorbers. We focused on structures which are highly absorbing for normally incident light and also exhibit highly directional absorptance. We optimized the layer thicknesses and materials using a genetic global optimization algorithm coupled to a transfer matrix code to maximize the angular selectivity in the absorptance at a single or multiple wavelengths.

We first considered structures composed of alternating layers of tungsten and silicon or silica over a tungsten substrate. We found that, due to the high absorption of tungsten, it is not possible to achieve angular selectivity in the absorptance with such structures. In addition, the absorptance of such tungsten-based structures is relatively broadband in nature, and is not associated with any strong resonances.

We next considered structures composed of alternating layers of silicon and silica. Unlike the tungsten-based multilayer structures, the optimized silicon-silica structures exhibit a resonance and high angular selectivity in absorptance at the wavelength at which they are optimized. The resonance is associated with large field enhancement in the structures. We also found that there is a trend of increasing angular selectivity as the number of layers increases. However, as the angular selectivity in absorptance increases, the wavelength range of high angular selectivity decreases.

We then considered optimizing the material composition of the multilayer structures, in addition to optimizing the layer thicknesses. For each layer, the material was chosen among silicon, silica, tungsten, and silicon carbide. Even though the optimized material composition was found to be, in general, different from the one of the silicon-silica multilayer structures, the improvement in angular selectivity with respect to silicon-silica structures with the same number of layers was marginal.

Finally, we investigated optimizing the absorptance of the multilayer structures at multiple wavelengths. We found that this approach leads to structures exhibiting almost perfect absorptance at normal incidence and narrow angular width in absorptance at these wavelengths. However, similar to the structures optimized at a single wavelength, the wavelength range of high angularly selective absorptance is narrow.

As final remarks, we note that due to the wavelength dependence of the dielectric permittivity of the materials utilized in the design, one cannot simply scale the layer thicknesses by a factor to scale the operating wavelength by that same factor. In other words, the optimized designs are not scale invariant, so the optimization process must be carried out at the new desired wavelength. It is also important to note that the optimized designs for the tungsten-silica and tungsten-silicon multilayer structures are non-unique. In other words, there are multiple designs which achieve the minimum fitness. On the other hand, the optimized designs for the silicon-silica multilayer structures are unique. In addition, we note that it is possible to design silicon-silica multilayer structures which exhibit high angular selectivity in absorptance at visible wavelengths without the tungsten substrate. In these structures, the light is absorbed in the silicon layers, since silicon is a lossy material in the visible.

It should also be noted that at the wavelength of $\lambda = 550$ nm the real part of the dielectric permittivity of tungsten is positive. Thus, at this wavelength tungsten behaves as an extremely lossy dielectric rather than as a plasmonic metal. The very high absorption of tungsten broadens all resonances both in angle and wavelength. In fact, we found that, if one assumes that tungsten is lossless [by setting $\epsilon_{tungsten} = \text{Re}(\epsilon_{tungsten})$ and neglecting the imaginary part $\text{Im}(\epsilon_{tungsten})$], then it is possible to design multilayer structures containing this artificially lossless tungsten which exhibit high angular selectivity in absorptance.

In addition, we note that the angular selectivity in absorptance can also be achieved by a structure consisting of a quarter-wave one-dimensional photonic crystal placed over a perfect mirror with an absorbing material included in the defect layer formed by the photonic crystal and the mirror. In the one-dimensional photonic crystal structure, the number of layers in the photonic crystal has to be adjusted in order to get unity absorptance at the resonance.[39] However, once the number of layers of the photonic crystal is chosen, the angular width of the absorptance cannot be tuned. Compared to such a structure, our proposed structures have many more degrees of freedom. Thus, it is possible to simultaneously obtain perfect absorptance on resonance and also tune the angular width of the absorptance. Our proposed aperiodic multilayer structures can achieve much narrower angular width than the one-dimensional photonic crystal

structures. In addition, with the proposed aperiodic structures it is possible to achieve perfect absorptance at normal incidence and narrow angular width in absorptance at multiple closely spaced tunable wavelengths. Such an absorptance response cannot be achieved with the one-dimensional photonic crystal structures.

ACKNOWLEDGMENTS

[1]W. Wang, Y. Cui, Y. He, Y. Hao, Y. Lin, X. Tian, T. Ji, and S. He, "Efficient multiband absorber based on one-dimensional periodic metal-dielectric photonic crystal with a reflective substrate," Opt. Lett. **39**, 331 (2014).

[2]D. Liang, Y. Huo, Y. Kang, K. X. Wang, A. Gu, M. Tan, Z. Yu, S. Li, J. Jia, X. Bao, S. Wang, Y. Yao, H. S. P. Wong, S. Fan, and J. S. Harris, "Optical absorption enhancement in freestanding GaAs thin film nanopyramid arrays," Adv. Energy Mater. **2**, 1254 (2012).

[3]E. Rephaeli and S. Fan, "Tungsten black absorber for solar light with wide angular operation range," Appl. Phys. Lett. **92**, 211107 (2008).

[4]N. Mattiucci, G. D'Aguanno, A. Alù, C. Argyropoulos, J. V. Foreman, and M. J. Bloemer, "Taming the thermal emissivity of metals: A metamaterial approach," Appl. Phys. Lett. **100**, 201109 (2012).

[5]J.-J. Greffet, R. Carminati, K. Joulain, J.-P. Mulet, S. Mainguy, and Y. Chen, "Coherent emission of light by thermal sources," Nature **416**, 61 (2002).

[6]Y. X. Yeng, J. B. Chou, V. Rinnerbauer, Y. Shen, S.-G. Kim, J. D. Joannopoulos, M. Soljacic, and I. Celanović, "Global optimization of omnidirectional wavelength selective emitters/absorbers based on dielectric-filled anti-reflection coated two-dimensional metallic photonic crystals," Opt. Express **22**, 21711 (2014).

[7]G. Veronis, R. W. Dutton, and S. Fan, "Metallic photonic crystals with strong broadband absorption at optical frequencies over wide angular range," J. Appl. Phys. **97**, 093104 (2005).

[8]G. C. R. Devarapu and S. Foteinopoulou, "Mid-IR near-perfect absorption with a SiC photonic crystal with angle-controlled polarization selectivity," Opt. Express **20**, 13040 (2012).

[9]T. Søndergaard and S. I. Bozhevolnyi, "Theoretical analysis of plasmonic black gold: periodic arrays of ultra-sharp grooves," New J. Phys. **15**, 013034 (2013).

[10]J. A. Schuller, T. Taubner, and M. L. Brongersma, "Optical antenna thermal emitters," Nat. Photonics **3**, 658 (2009).

[11]J. Hao, L. Zhou, and M. Qiu, "Nearly total absorption of light and heat generation by plasmonic metamaterials," Phys. Rev. B **83**, 165107 (2011).

[12]O. Stenzel, A. Stendal, K. Voigtsberger, and C. von Borczyskowski, "Enhancement of the photovoltaic conversion efficiency of copper phthalocyanine thin film devices by incorporation of metal clusters," Sol. Energy Mater. Sol. Cells **37**, 337 (1995).

[13]M. Westphalen, U. Kreibig, J. Rostalski, H. Lüth, and D. Meissner, "Metal cluster enhanced organic solar cells," Sol. Energy Mater. Sol. Cells **61**, 97 (2000).

[14]E. Rephaeli and S. Fan, "Absorber and emitter for solar thermophotovoltaic systems to achieve efficiency exceeding the Shockley-Queisser limit," Opt. Express **17**, 15145 (2009).

[15]S. Y. Lin, J. Moreno, and J. G. Fleming, "Three-dimensional photonic-crystal emitter for thermal photovoltaic power generation," Appl. Phys. Lett. **83**, 380 (2003).

[16]S. Y. Lin, J. G. Fleming, Z. Y. Li, I. El-Kady, R. Biswas, and K. M. Ho, "Origin of absorption enhancement in a tungsten, three-dimensional photonic crystal," J. Opt. Soc. Am. B **20**, 1538 (2003).

[17]A. K. Sharma, S. H. Zaidi, P. C. Logofatu, and S. R. J. Brueck, "Optical and electrical properties of nanostructured metal-silicon-metal photodetectors," IEEE J. Quantum Electron. **38**, 1651 (2002).

[18]H. Huang, Y. Huang, X. Wang, Q. Wang, and X. Ren, "Long wavelength resonant cavity photodetector based on InP/air-gap Bragg reflectors," IEEE Photonics Technol. Lett. **16**, 245 (2004).

[19]A. Tittl, P. Mai, R. Taubert, D. Dregely, N. Liu, and H. Giessen, "Palladium-based plasmonic perfect absorber in the visible wavelength range and its application to hydrogen sensing," Nano Lett. **11**, 4366 (2011).

[20]N. Liu, M. Mesch, T. Weiss, M. Hentschel, and H. Giessen, "Infrared perfect absorber and its application as plasmonic sensor," Nano Lett. **10**, 2342 (2010).

[21]M. Diem, T. Koschny, and C. M. Soukoulis, "Wide-angle perfect absorber/thermal emitter in the terahertz regime," Phys. Rev. B **79**, 033101 (2009).

[22]J. Hendrickson, J. Guo, B. Zhang, W. Buchwald, and R. Soref, "Wideband perfect light absorber at midwave infrared using multiplexed metal structures," Opt. Lett. **37**, 371 (2012).

[23]C. Hu, Z. Zhao, X. Chen, and X. Luo, "Realizing near-perfect absorption at visible frequencies," Opt. Express **17**, 11039 (2009).

[24]T. V. Teperik, F. J. Garcia de Abajo, A. G. Borisov, M. Abdelsalam, P. N. Bartlett, Y. Sugawara, and J. J. Baumberg, "Omnidirectional absorption in nanostructured metal surfaces," Nat. Photonics **2**, 299 (2008).

[25]K. Aydin, V. E. Ferry, R. M. Briggs, and H. A. Atwater, "Broadband polarization-independent resonant light absorption using ultrathin plasmonic super absorbers," Nat. Commun. **2**, 517 (2011).

[26]M. K. Hedayati, M. Javaherirahim, B. Mozooni, R. Abdelaziz, A. Tavassolizadeh, V. S. K. Chakravadhanula, T. Strunkus, F. Faupel, and M. Elbahri, "Design of a perfect black absorber at visible frequencies using plasmonic metamaterials," Adv. Mater. **23**, 5410 (2011).

[27]Y. Cui, K. H. Fung, J. Xu, H. Ma, Y. Jin, S. He, and N. X. Fang, "Ultrabroadband light absorption by a sawtooth anisotropic metamaterial slab," Nano Lett. **12**, 1443 (2012).

[28]T. Søndergaard, S. M. Novikov, T. Holmgaard, R. L. Eriksen, J. Beermann, Z. Han, K. Pedersen, and S. I. Bozhevolnyi, "Plasmonic black gold by adiabatic nanofocusing and absorption of light in ultra-sharp convex grooves," Nat. Commun. **3**, 969 (2012).

[29]G. C. R. Devarapu and S. Foteinopoulou, "Broadband mid-IR superabsorption with aperiodic polaritonic photonic crystals," J. Eur. Opt. Soc.: Rapid Public. **9**, 14012 (2014).

[30]C. Argyropoulos, K. Q. Le, N. Mattiucci, G. D'Aguanno, and A. Alù, "Broadband absorbers and selective emitters based on plasmonic Brewster metasurfaces," Phys. Rev. B **87**, 205112 (2013).

[31]Y. Shen, D. Ye, Z. Wang, L. Wang, I. Celanović, L. Ran, J. D. Joannopoulos, and M. Soljačić, "Metamaterial broadband angular selectivity," Phys. Rev. B **90**, 125422 (2014).

[32]M. Florescu, H. Lee, I. Puscasu, M. Pralle, L. Florescu, D. Z. Ting, and J. P. Dowling, "Improving solar cell efficiency using photonic band-gap materials," Sol. Energy Mater. Sol. Cells **91**, 1599 (2007).

[33]P. Bermel, M. Ghebrebrhan, M. Harradon, Y. X. Yeng, I. Celanović, J. D. Joannopoulos, and M. Soljačić, "Tailoring photonic metamaterial resonances for thermal radiation," Nanoscale Res. Lett. **6**, 549 (2011).

[34]Y. Shen, D. Ye, I. Celanović, S. G. Johnson, J. D. Joannopoulos, and M. Soljačić, "Optical broadband angular selectivity," Science **343**, 1499 (2014).

[35]I. Celanović, F. O'Sullivan, M. Ilak, J. Kasaakian, and D. Perreault, "Design and optimization of one-dimensional photonic crystals for thermophotovoltaic applications," Opt. Lett. **29**, 863 (2004).

[36]C. H. Granier, F. O. Afzal, C. Min, J. P. Dowling, and G. Veronis, "Optimized aperiodic highly directional narrowband infrared emitters," J. Opt. Soc. Am. B **31**, 1316 (2014).

[37]C. M. Cornelius and J. P. Dowling, "Modification of Planck blackbody radiation by photonic band-gap structures," Phys. Rev. A **59**, 4736 (1999).

[38]*CRC Handbook of Chemistry and Physics*, 88th ed., edited by D. R. Lide (CRC Press, Boca Raton, 2007).

[39]I. Celanovic, D. Perreault, and J. Kassakian, "Resonant-cavity enhanced thermal emission," Phys. Rev. B **72**, 075127 (2005).

[40]D. E. Goldberg and K. Deb, "A comparative analysis of selection schemes used in genetic algorithms," in *Foundations of Genetic Algorithms*, edited by G. J. E. Rawlins (Morgan Kaufmann, San Francisco, 1997), p. 69.

[41]K. Krishnakumar, "Micro-genetic algorithms for stationary and non-stationary function optimization," Proc. SPIE **1196**, 289 (1990).

[42]K. Deb and S. Agrawal, "Understanding interactions among genetic algorithm parameters," in *Foundations of Genetic Algorithms*, edited by W. Banzhaf and C. Reeves(Morgan Kaufmann, San Francisco, 1999), p. 268.

[43]D. E. Goldberg, K. Deb, and J. H. Clark, "Genetic algorithms, noise, and the sizing of populations," Complex Syst. **6**, 333 (1992).